

Ultrafast pulse shaping: amplification and characterization

M.R. Fetterman, D. Goswami, D. Keusters, W. Yang, J.-K. Rhee and W.S. Warren

Princeton University Center for Ultrafast Laser Applications
Princeton University, Princeton NJ 08544

fetterma@princeton.edu, debu@chemvax.princeton.edu, keusters@princeton.edu,
wgyang@ee.princeton.edu, rheej@corning.com, wwarren@princeton.edu

Abstract. We demonstrate high-resolution amplified pulse shaping using an acousto-optic modulator (AOM) at a center-wavelength of 795nm. The output pulses have energy of 200 μ J/pulse and a transform-limited pulsewidth of 150fs. A spectral modulation of over 40 features is achieved in a single pulse. We characterize the pulses using the STRUT (Spectrally and Temporally Resolved Upconversion Technique). Using predistortion techniques, we demonstrate that the pulses can be shaped in amplitude and phase. We create a complex pulse shape with hyperbolic secant amplitude and hyperbolic tangent frequency sweep, which is useful for applications in adiabatic rapid passage experiments.

©1998 Optical Society of America

OCIS codes: (320.0320) Ultrafast Optics; (320.5540) Pulse Shaping; (320.7100) Ultrafast Measurements

References

1. J.S. Melinger, S.R. Gandhi, W.S. Warren, "Adiabatic Population Transfer with Frequency Swept Laser Pulses," *J. Chem. Phys.* **101**, 6439 (1994).
2. L. Allen, J. Eberly, *Optical Resonance and Two-Level Atoms* (Dover Publications, 1987).
3. D. Goswami, *Control of Chemical Dynamics Using Arbitrarily Shaped Optical Pulses and Laser Enhanced NMR Spectroscopy*, *PhD. Thesis*, (Princeton University, 1994).
4. J.X. Tull, M.A. Dugan, C.W. Hillegas, W.S. Warren, "Robust Pulse Shaping Techniques for Quantum Molecular Control," *Ultrafast Phenomena IX*, G.A. Mourou and A.H. Zewail, eds. (Springer-Verlag, Berlin, 1995).
5. J.X. Tull, M.A. Dugan, W.S. Warren, "High Resolution Acousto-Optic Shaping of Unamplified and Amplified Femtosecond Laser Pulses," *J. Opt. Soc. B* **14**, 2348 (1997).
6. J.X. Tull, *The Development of High Resolution Ultrafast Pulse Shaping Techniques*, *PhD. Thesis*, (Princeton University, 1996).
7. M.M. Wefers, K.A. Nelson, A.M. Weiner, "Multi-Dimensional Femtosecond Pulse Shaping," *Ultrafast Phenomena X*, P. F. Barbara, J. G. Fujimoto, W. H. Knox and W. Zinth, eds. (Springer-Verlag, Berlin, 1996).
8. A.M. Weiner, D.E. Learid, J.S. Patel, J.R. Wullert, "A Programmable Shaping of Femtosecond Optical Pulses by use of 128-element liquid-crystal phase modulator," *J. Quantum Electron.*, **28**, 908-920 (1992).
9. D. Strickland, G. Mourou, "Compression of Amplified Chirped Optical Pulses," *Opt. Commun.* **58**, 219 (1985).
10. J.-K. Rhee, T.S. Sosnowski, A.-C. Tien, and T.B. Norris, "Real-Time Dispersion Analyzer of Femtosecond Laser Pulses with Use of a Spectrally and Temporally Resolved Upconversion Technique," *J. Opt. Soc. Am. B* **13** 1780-1785.
11. J.-K. Rhee, T.S. Sosnowski, T.B. Norris, J.A. Arns, W.S. Colburn, "Chirped-Pulse Amplification of 85-fs Pulses at 250 KHz with 3rd-Order Dispersion Compensation by use of Holographic Transmission Gratings," *Opt. Lett.* **19**, 1550-1552 (1994).
12. J.P. Foing, J.P. Likforman, M. Joffe, A. Migus, "Femtosecond Pulse Phase Measurement by Spectrally Resolved Up-Conversion- Application to Continuum Compression," *J. Quantum Electron.* **28**, 2285-2290 (1992).
13. Coherent Lasers, <http://www.cohr.com>, Santa Clara, Ca.
14. Clark-MXR Inc., <http://www.clark-mxr.com>, Dexter, MI.

15. Brimrose Corporation of America, <http://www.brimrose.com>, Baltimore, MD.
 16. LeCroy Corporation, <http://www.lecroy.com>, Chestnut Ridge, NY.
 17. M.R. Fetterman, *Demonstration of an Amplified Pulse Shaping System, and its Applications to Adiabatic Rapid Passage*, *PhD. Thesis*, (Princeton University, 1999).
 18. W. Yang, F. Huang, M.R. Fetterman, D. Goswami, W.S. Warren, "Demonstration of Amplitude Feedback in an Ultrafast Pulse Shaping System at 1.55 μ m," *Opt. Lett.* (1999) (to be published).
 19. W. Yang, J. Davis, D. Goswami, M.R. Fetterman, W.S. Warren, "Optical wavelength domain code-division multiplexing using AOM-base ultrafast optical pulse shaping," *All-Optical Networking: Architecture, Control, and Management Issues*, SPIE Vol. 353 (1998).
 20. M.R. Fetterman, D. Goswami, D. Keusters, J.-K Rhee, W.S. Warren, "Generation of Amplified Shaped Pulses for Highly Adiabatic Excitation," *Ultrafast Phenomena IX*, G.A. Mourou and A.H. Zewail, eds.(Springer-Verlag, Berlin, 1995).
-

I. Introduction

Shaped high-energy pulses can generate population inversion efficiently, and thus are useful in diverse applications such as quantum computing and laser selective chemistry. In general, the standard Gaussian pulse output from an amplified short-pulse laser system cannot generate population inversion even in a two-level system. The Rabi frequency inhomogeneities that can arise from spatial variations in laser intensity or a number of other effects make it difficult to achieve complete inversion within the dephasing time of the target system [1]. By shaping the pulse, it is possible to create population inversion through adiabatic rapid passage [2], which can lead to a very robust yet selective inversion over a wide range of intensities and frequencies [3, 4].

Previous programmable pulse shaping demonstrations [4, 5, 6, 7, 8] have not achieved power levels that are required for many applications, such as selective population transfer, driving non-linear processes, etc. In our present work, we implement ultrafast pulse shaping with a commercially available femtosecond chirped pulse amplification (CPA) [9] system and demonstrate high-energy shaped pulses. We use the AOM (acousto-optic modulator) technique developed in our group to achieve the shaped pulses [4, 5, 6].

We demonstrate high resolution shaping in both amplitude and phase domains using predistortion to compensate for errors. We generate complex waveforms, such as the hyperbolic secant amplitude pulse with hyperbolic tangent frequency sweep. We use STRUT [10, 11, 12], which has been used previously to characterize pulses from CPA laser systems, as the characterization technique

II. Experimental Setup

The system layout is shown schematically in Fig.1, with the AOM pulse shaper inserted into a commercially available femtosecond Ti:sapphire oscillator and regenerative amplifier system. The oscillator (MIRA, Coherent [13]) is pumped with 8W at 514nm from a cw argon-ion laser (INNOVA 400, Coherent [13]) to produce 110-fs pulses at a center wavelength of 795nm. A typical spectral bandwidth of 10nm is measured at the FWHM (full width at half maximum). Each oscillator pulse has energy of approximately 13nJ at a repetition rate of 76MHz.

The oscillator output pulses are then injected to the Ti:sapphire regenerative amplifier (Clark/MXR [14]) through the AOM pulse shaper to produce shaped and amplified pulses with 200 μ J energy per pulse. The amplifier uses the CPA technique and is pumped with a Q-switched frequency-doubled Nd:YAG at a repetition rate that was set to 1kHz, but can be set up to 50kHz. By the CPA scheme, oscillator pulses (without shaping) are stretched to 150ps, amplified and compressed to 150fs with 200 μ J energy per pulse. The bandwidth is reduced to 8nm due to gain-bandwidth narrowing. It is important to stretch the pulses

adequately because otherwise nonlinear effects will distort the shaped pulse in the regenerative amplifier.

The AOM pulse shaping technology has been described in detail in previous work [4, 5, 6], and consists of a zero-dispersion line and an AOM (Brimrose, [15]) as shown schematically in Fig. 1. The broad spectrum of a femtosecond pulse is dispersed spatially by

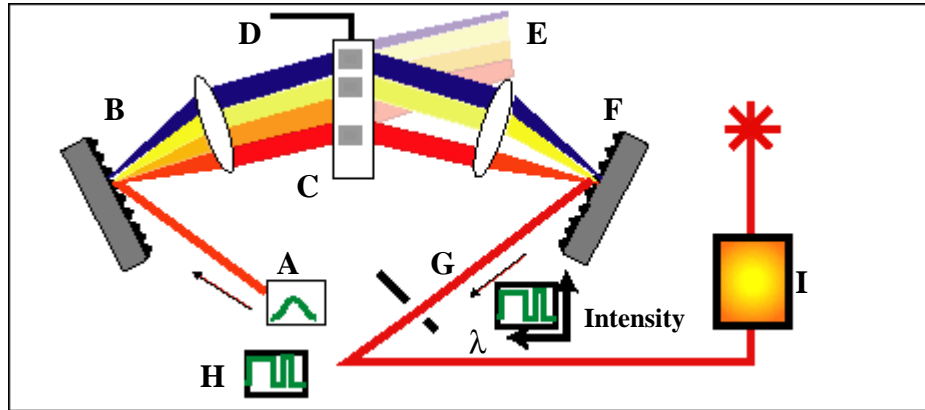


Fig. 1. Schematic of the AOM pulse shaping system. The femtosecond Gaussian pulse (plotted as a function of time in the box below A) is the input pulse on the left side of the figure. The grating B spectrally spreads the pulse. The acousto-optic modulator C is in the center of the system. The RF-wave D propagates through the AOM, creates a spatial mask inside the crystal and shapes the optical pulse. In this schematic, we have modeled the input optical pulse as consisting of four different wavelengths, blue, yellow, orange, and red, which would represent a 4-bit system. In principle, the AOM is capable of shaping 1000 bits. The undiffracted beam E passes out of the system. The white parts of the diffracted spectrum are left undiffracted by the AOM. The spectrum recombines in grating F. The output (G and the box below the G) shows the shaped output pulse as a function of wavelength. As the rf wave propagates, different shapes are created. The pulse picker G picks the pulse at the correct time out of the pulse train. Here the pulse picker is shown separately selecting a particular pulse H, but in the experiment, the pulse picker is located inside the regenerative amplifier I.

1800lines/mm gratings. It is then collimated with a 30-cm lens to form a linear spectral image at the center (referred to as point C in Fig.1) of the 4-F system. Shaped RF (radio frequency) pulses create the desired modulation pattern on the AOM, which is placed at the point C. The shaped RF pulses [6] are generated by an arbitrary function generator (LeCroy, [15]) with a resolution of 400MHz is used. In this particular system, a tellurium-dioxide (TeO_2) crystal is used in the AOM. The acoustic velocity of $4.2\text{mm}/\mu\text{s}$ in TeO_2 is far slower than the speed of light, and consequently, with respect to the light pulse, the acoustic wave may be considered stationary. Thus, the acoustic wave acts as a transmission diffraction grating [6]. The AOM has $40 \times 2.3\text{mm}^2$ clear aperture size. The full width at half maximum on the spectrum is approximately 30mm on the AOM.

The pulse shaper is inserted into the system as shown in Fig.1, before the regenerative amplifier. It would also be possible to place the pulse shaper in the regenerative amplifier, or after the regenerative amplifier. The option of putting the pulse shaper in the regenerative amplifier would require a complete redesign of the amplifier. By not modifying the amplifier, we make the pulse shaper a device that can be used with existing technology. There are clear advantages of putting the pulse shaper before the regenerative amplifier, rather than after. For example, assume that the regenerative amplifier has an output power of P_0 . The pulse shaping system has a low efficiency of about $E=5\text{-}10\%$. The regenerative amplifier is a saturated amplifier, which means that even if the power into the amplifier is low, the output power will still be P_0 . However, if we put the pulse shaper after the amplifier, the system output power

will be reduced to $P_0 \times E$. In the arrangement where the pulse shaper is before the amplifier, caution is required not to seed a narrow band pulse into the stretcher so as not to damage the amplifier.

In order to characterize the pulse shaper before amplification, we used a Ronchi grating with dark lines spaced equally at a distance of about 50 microns. The AOM was replaced by the Ronchi grating. Unlike the AOM, the Ronchi grating does not change with time. Thus, using the Ronchi grating allowed us to study the zero-dispersion line without using the amplifier or a pulse picker. The output from the shaper is analyzed with a spectrometer. The result of this experiment showed us that the amplifier did not distort the high-contrast, high-resolution pulses generated by the pulse shaper. The resolution is higher than the resolution of our measurement device, a spectrometer, which has a resolution of 0.3nm. When the pulse is shaped with features of 0.3nm, the measured contrast ratio is 12dB, which is also lower than the actual value because of the spectrometer resolution. At lower pulse shaping resolutions, we measure a contrast ratio that is higher than 20dB. In fact, the acousto-optic modulator performs as well as the Ronchi grating, and data to show the pulse shaping resolution and contrast ratio is shown in the next section of this paper.

When the AOM is used, it is necessary to select only one pulse at the correct timing because the acoustic wave features travel across the AOM, as shown in Fig.1. This means that each pulse will see a different grating function on the modulator. The Pockels-cell cavity dumper is capable of injecting only one pulse into the regenerative amplifier at the right timing, so that we can obtain a desired pulse shape.

The spectrometer only gives amplitude as a function of wavelength, while the time-domain correlation gives information of group delay, hence the temporal information. The STRUT [10, 11, 12] recovers both the amplitude and phase information. It can be viewed as a time-domain correlator that is also resolved in wavelength. An important feature of the STRUT is that the algorithm is fast and does not require iteration. It can also give the sign of the chirp. We use a STRUT with a time scanning configuration [11].

III. Calibration of the Pulse Shaper

The pulse shaper shapes the optical pulse through the interaction of the acoustic wave with the RF wave, which is described mathematically as a transfer function. The amplified Ti:sapphire laser pulse is expressed as $E_{in}(\omega)$, the pulse shaper transfer function as $M(\omega)$, and the output measured pulse as $E_{out}(\omega)$. In this paper we will always use ω to refer to the frequency of the optical pulse, and not the frequency of the rf pulse. Ignoring nonlinear effects in the pulse shaping system, such as distortions by the regenerative amplifier, we may write [6]:

$$E_{out}(\omega) = M(\omega)E_{in}(\omega) \quad (1)$$

When $M(\omega)=1$, corresponding to no modulation of the RF wave, we will measure the pulse $E_{in}(\omega)$. Effects such as distortions in the regenerative amplifier will be included in $E_{in}(\omega)$. To produce a desired pulse shape $D(\omega)$, such as the rectangular pulse, we apply the pulse shape function given by $M_1(\omega)$ or $M_2(\omega)$:

$$M_1(\omega) = D(\omega)E_{in}(\omega)^{-1} \quad (2a)$$

$$M_2(\omega) = D(\omega)|E_{in}(\omega)|^{-1} \quad (2b)$$

Eq. (2) describes an experiment where we measure the experimental waveform $E_{in}(\omega)$, and use it to calculate the appropriate pulse shaper function. We refer to this as predistortion. In this paper, the spectrometer is used to make the measurement of $|E_{in}(\omega)|$, and so Eq.(2b) is appropriate. The phase sensitive predistortion described in Eq.(2a) requires a detection device such as the STRUT, and has been demonstrated in other work [17]. If the predistortion of Eq.(2b) is implemented in a continuous loop, it will then be a feedback system [18].

The acoustic wave propagates across the AOM such that there is a linear relationship between the RF time and the optical frequency, with the constant determined by parameters of the pulse shaping system such as the geometry of the pulse shaper and the speed of sound in the AOM crystal. This relationship between RF time and optical frequency is given by:

$$M(\omega) = f(t_{RF} = \alpha\omega) \quad (3)$$

In practice, both α and $E_{in}(\omega)$ are determined experimentally. Once these are determined, the pulse shaper is calibrated, and arbitrary pulse shapes may be produced.

The value of α is determined from the experimental data set of Fig.2. Each line in Fig.2A represents the spectrum that is a result of sending a short RF pulse into the AOM at different RF time delays. The same data set is shown in a contour plot in Fig.2B. The data of Fig.2B was linearly fit (red line, Fig.2B) according to Eq.(3) to find that $\alpha = -126.98 \mu\text{s}/\omega_0$, where the central optical angular frequency is given by $\omega_0 = 2.37 \times 10^{15} \text{Hz}$, corresponding to $\lambda = 795 \text{nm}$. Equivalently, in wavelength space, Fig.2B shows that $0.5 \mu\text{s}$ corresponds to 3.125nm . We can then use the AOM to create desired phase modulations using the quantity α that is found from the data of Fig.2. The measured pulse amplitude, $|E_{in}(\omega)|$, can also be found from the data of Fig.2A. Thus, using Fig.2A, the AOM system is calibrated in optical wavelength and RF time.

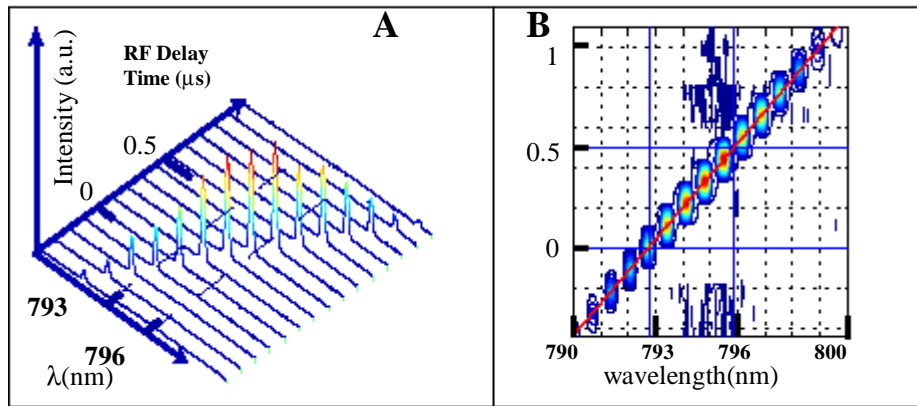


Fig. 2. Calibration curves for AOM pulse shaper. **A.** Each line in this figure represents a different optical spectrum. Application of a short RF pulse with a different delay time into the AOM created each spectrum. The different delay time corresponds to a different spatial position on the AOM and therefore a different spectral position. By using this figure, we can calibrate the pulse-shaper response-function with respect to amplitude and time. **B.** The data from **A** is viewed as a contour plot. The solid red line fits the data so that we can calibrate the RF time with respect to optical wavelength.

III. Experimental Results

In this section, we will demonstrate the results from the pulse shaping experiments in the wavelength and temporal domains. To fit this data, we use the calibration from the previous section.

In Fig.3, we show an example of high-resolution pulse shaping. In Fig.3A (upper), we show a data stream with 43 bits:

$$\Psi = [0110 \ 0111 \ 1101 \ 1100 \ 1110 \ 1011 \ 1000 \ 1111 \ 0011 \ 1100 \ 111] \quad (4)$$

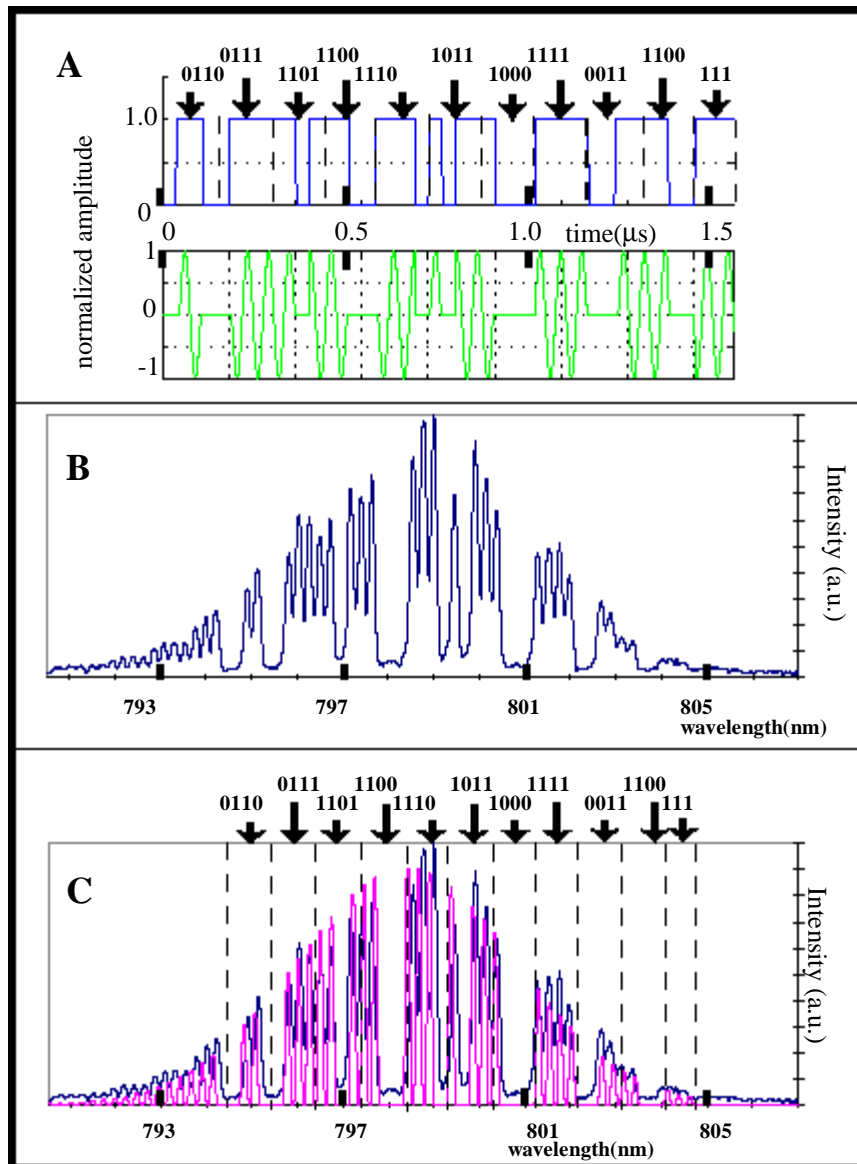


Fig. 3. High Resolution Pulse Shaping. **A.** The RF signal used to modulate the spectrum. (top) The bit stream, which is given as Eq.(4) in the text. The numbers show the imposed bit pattern, a 43 bit sequence. The lower figure shows that the actual RF signal was the product of this bit stream with a sinusoidal wave. **B.** The spectrum resulting from the modulated RF signal of A. **C.** This shows the data of B (blue), with a theoretical fit (magenta). The fit shows that we have recovered the 43 bits imposed upon the spectrum. The numbers at the top of this figure correspond to those in A.

Fig.3A (lower) shows the actual RF waveform that we applied, which was the product of the data stream with a sinusoidal wave. Fig.3B shows the modulated spectrum that results from applying this RF pulse. With no modulation, the spectrum of Fig.3B would simply be the smooth Gaussian, $E_{in}(\omega)$. In Fig.3C, we show this same data set (blue), along with a theoretical fit (magenta) derived from Eq.(2b).

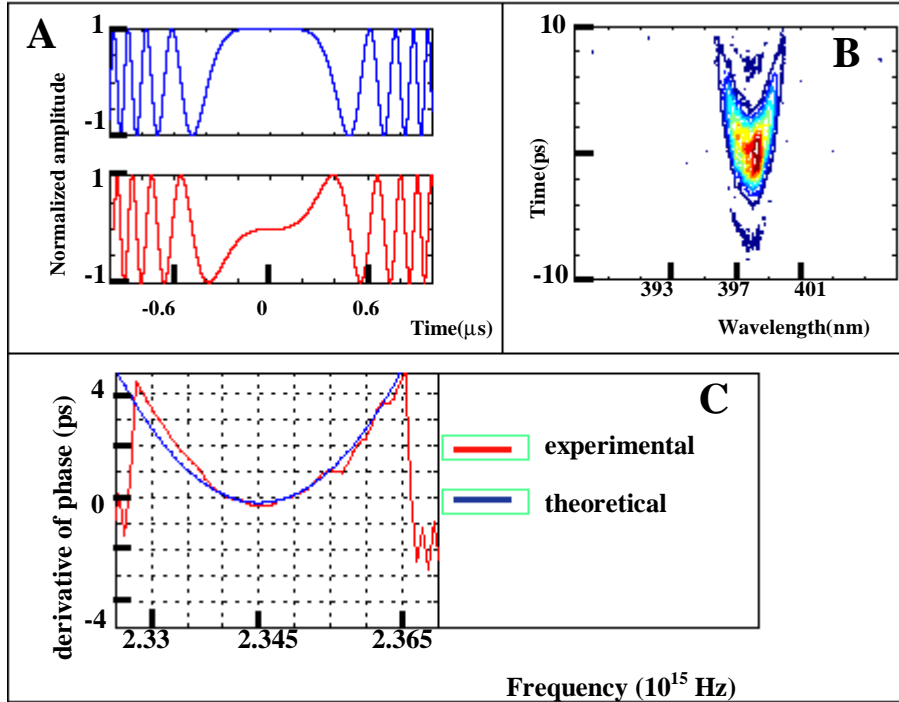


Fig.4 **A.** The RF pulses that are used to create an optical pulse with cubic phase, $g_{(RF)} = \exp[i(\beta t)^3]$. The blue curve is the real part and the red curve is the imaginary part. **B.** STRUT image of a pulse with cubic phase. The x-axis shows wavelength and the y-axis shows time. **C.** The red curve shows the recovered phase derivative $d\phi/d\omega$ from the STRUT image. The blue curve is the theoretically predicted result, using the data from Fig.2 and the RF signals of Fig.4A as input parameters.

The data of Fig.3 represents a preliminary demonstration of pulse shaping as applied to communication, which has been studied in more detail [19]. This data was taken during the early stages of the system development, and the contrast ratio is not as high as in later work. In this case, the Ti:sapphire laser was tuned to a different center wavelength. The Ti:sapphire center wavelength may be tuned over 25nm with only minor adjustments to the pulse shaper such as changing the angle of the pulse shaper diffraction gratings [17].

In Fig.4, we analyze the parameters of a pulse with cubic phase using the STRUT technique. Fig.4A shows the input RF pulse to the AOM, given by $f(t_{RF}) = \exp[i(\beta t)^3]$, with $\beta = 3$ and t in μs . The top curve, in blue, is the real part of the RF pulse, $x = \cos[(\beta t)^3]$, while the bottom curve, in red, is the imaginary part, $y = \sin[(\beta t)^3]$. In this case we are modulating only the phase and not the pulse amplitude. This RF pulse will give an optical pulse:

$$E_{out}(\omega) = \exp[i[\alpha\beta(\omega - \omega_0)]^3] E_{in}(\omega) \quad (5)$$

Fig.4B shows the experimental STRUT image resulting from this RF pulse. The red line in Fig.4C shows the derivative of the phase $d\phi/d\omega$ that is recovered from this STRUT image and the blue line shows the theoretically predicted phase derivative from Eq.(5). In this theoretical fit, we assume a Gaussian with constant phase for $E_{in}(\omega)$.

The cubic phase pulse is an example of shaping the pulse with a RF wave that was determined without prior knowledge of the optical pulse shape. As described in Section II, for many cases it will be useful to apply predistortion.

In Fig.5, we demonstrate predistortion as described in Eq.(2b). Fig.5a shows an optical spectrum, which uses the lower x-axis as the wavelength scale, and the RF pulses,

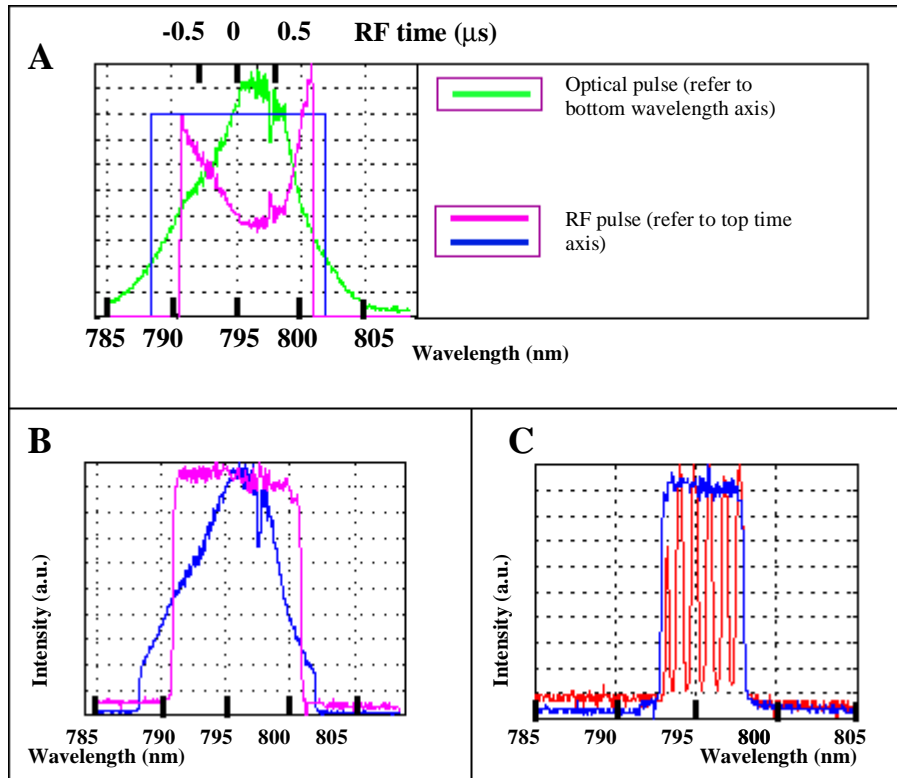


Fig.5. Predistortion. **A.** This figure has two x-axis: the lower wavelength x-axis is for the green curve and the upper RF time axis is for the blue and magenta curves. The original gaussian pulse (green color, optical spectrum) which has a somewhat distorted shape is shown. The blue square pulse in Fig.5A is a RF pulse. The magenta curve is a RF wave, calculated from Eq. (2), that will create an optical square pulse. **B.** These are all optical spectra. Blue curve: the clipped wave, generated by sending in the blue rf pulse of Fig.5A. Magenta curve: square pulse that is actually wider than the natural response of the system. **C.** Blue curve: another square wave, which is square to within 90%. Red curve shows modulation of this square wave.

which use the upper x-axis as their time-scale. These curves show how the predistorted RF pulses are calculated from the optical spectra. The original optical spectrum (green color) is a distorted gaussian with a FWHM of 7nm. The blue square pulse in Fig.5A is a RF pulse, with an arbitrary intensity scale. The magenta curve of Fig.5A is a RF wave, calculated from Eq.(2b) that will create an optical square pulse. Note that it is small in the center, where the optical pulse (green) is maximum, and largest in the wings, where the optical pulse is minimum. In Fig.5B, we show the results of this predistortion.

The blue curve in Fig.5B shows the spectrum that results from the RF pulse of Fig.5A (blue). The magenta curve shows the square optical wave that is generated using the magenta curve in Fig.5A. The square optical pulse is square to within 90% with this technique. The accuracy could be improved by using a feedback system [16], instead of just the single iteration that is performed here. Note that we have extended the amplification to the wings in the spectrum, and produced a square pulse with 10nm width (Fig.5B, magenta curve). This width is even broader than that of our original pulse. In Fig.5C we show another square pulse, with a narrower bandwidth (blue curve). The square pulse can then be modulated with additional features (Fig.5C, red curve), which demonstrates the high resolution of this system and the versatility of the predistortion scheme.

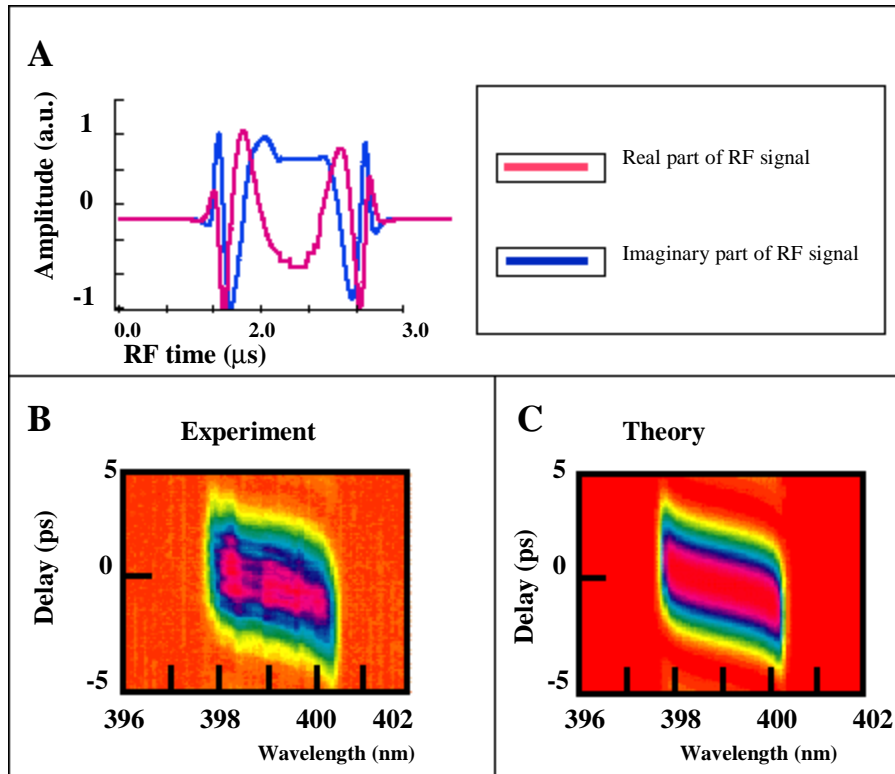


Fig.6 Results for hyperbolic secant amplitude with hyperbolic tangent frequency sweep pulse. **A.** RF signal used to create sec+ pulse. **B.** STRUT trace (experimental). **C.** STRUT trace (theoretical).

In Fig.6, using all these techniques discussed above, we demonstrate the generation and characterization of a complex pulse shape, the hyperbolic secant pulse with hyperbolic tangent frequency sweep, given by:

$$E(t) = \text{sech}(\rho t)^{(1+\mu)} \quad (6)$$

Eq.(6) describes the optical pulse, where $\rho = 1.5 \times 10^{12}$ Hz is a time width parameter and t is the pulse time in sec. With the frequency sweep parameter μ given by $\mu = +10$, we will refer to this pulse as the sec+ pulse. Generation of the sec+ pulse requires phase modulation, which was shown in Fig.4, and amplitude predistortion as shown in Fig.5.

To find the RF pulse corresponding to this complex pulse shape, we first take the Fourier transform of the optical pulse to express it in the frequency domain. Then, the correspondence between RF time and optical frequency is used, as given in Eq.(3). Fig.6A (upper) shows the real (red curve) and imaginary (blue curve) parts of the RF signal used to generate this complex pulse shape. After generating the RF pulse with Eq.(2b), we then measured the output pulse, and slightly modified the RF pulse to give a pulse shape that would be closer to the desired sec+ pulse shape. This process represents a multiple iteration of predistortion, and may be necessary because of nonlinear effects in the pulse shaping system [17]. Fig.6B shows the STRUT trace of the sec+ pulse. In Fig.6C, the theoretical STRUT trace, generated from Eq.(6) is shown. It resembles the experimental result closely.

In Fig.7, the data from Fig.6B is analyzed. In Fig.7A, the derivative of the phase (green) is shown, along with the theoretical phase derivative (red) from Eq.(6). The theoretical intensity (blue) is shown, and it can be seen that the experimental and theoretical phase derivatives agree well in the region where the intensity is significant. Fig.7B shows the

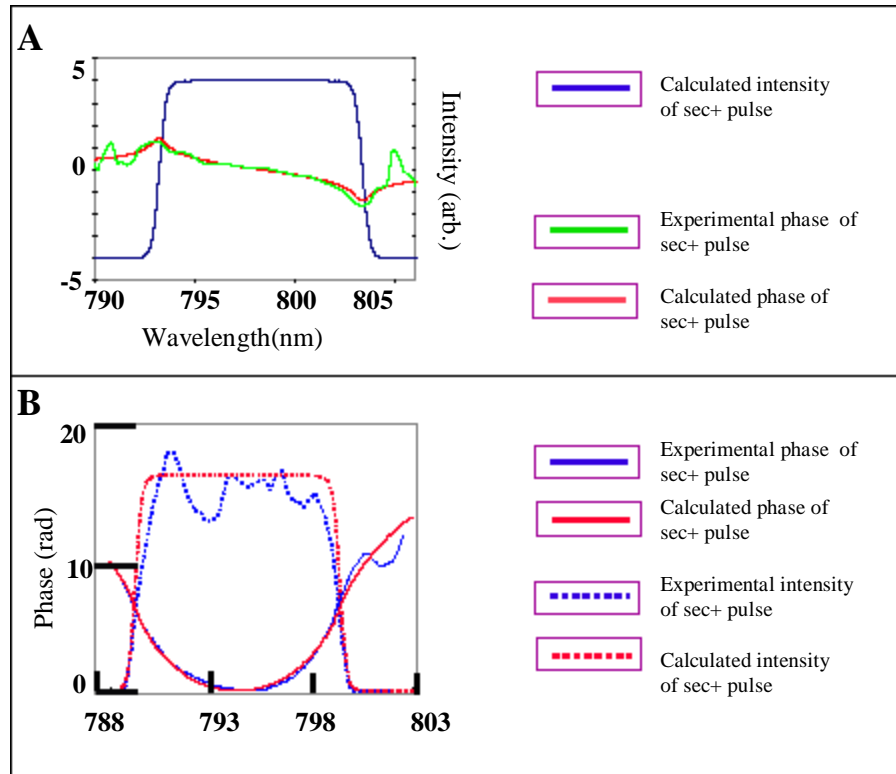


Fig.7 Analysis of STRUT data of Fig.6B. **A.** Derivative of the phase, both theoretical and experimental. The theoretical intensity is also shown. **B.** Intensity and phase, both theoretical and experimental.

intensity (blue dotted line) and phase (blue) that are recovered from the STRUT of Fig.6B, as well as the theoretical intensity (red dotted line) and phase (red).

This pulse has applications to adiabatic excitation of atomic levels [2], and we have shown that it has intriguing effects on atomic systems [20]. Assume that there is a two level system with resonance at the center frequency of the pulse, ω_0 . The y-axis of Fig.7A can be viewed as time. Fig.7A shows that the pulse spends a long time at frequencies that are detuned from the resonance frequency ω_0 , then quickly sweeps through resonance, and then slowly increases in frequency. This temporal behavior is characteristic of the hyperbolic secant pulse with hyperbolic tangent frequency sweep, and is one of the very few analytical solution for adiabatic rapid passage [2].

IV. Conclusions and Acknowledgements

In this paper, we have demonstrated a shaped amplified pulse system with an output power of $200\mu\text{J}/\text{pulse}$. The cubic phase pulse demonstrates that the pulses can be shaped in the phase domain. Using predistortion techniques, we have shown the pulse can be modified to a desired shape in the amplitude domain with high resolution and contrast ratio. We have also used the STRUT to fully characterize the pulse in amplitude and phase. The combination of the STRUT and the pulse shaper fully demonstrates the capabilities of amplified pulse shaping. The hyperbolic secant pulse with hyperbolic tangent frequency sweep is shown, which will have applications to adiabatic rapid passage experiments.

We thank Xinjie Zhang for his contributions, and the reviewers for their helpful comments. This work is supported by the National Science Foundation and the New Jersey Commission on Science and Technology.